The Astronomical Journal, 156:115 (11pp), 2018 September https://doi.org/10.3847/1538-3881/aad3d1
© 2018. The American Astronomical Society. All rights reserved.

A Multicolor Study of Polarization Variability in Isolated B[e] Stars HD 45677 and HD 50138

C. D. Lee[1], C. Eswaraiah[1,2,3], W. P. Chen[1,4], and A. K. Pandey[2]
[1] Graduate Institute of Astronomy, National Central University, 300 Jhongda Road, Jhongli 32001, Taiwan
[2] Aryabhatta Research Institute of Observational Sciences, Manora Peak, Nainital 263129, India
[3] Institute of Astronomy, National Tsing-Hua University (NTHU), Hsinchu 30013, Taiwan
[4] Department of Physics, National Central University, 300 Jhongda Road, Jhongli 32001, Taiwan
Received 2018 June 25; accepted 2018 July 13; published 2018 August 23

Abstract

HD 45677 and HD 50138 are two B[e] stars isolated from any known star-forming regions. We investigated the polarization characterization of their surrounding gas and in situ dust in the inner edge of the circumstellar disk. Our measurements of the intrinsic polarization of each star between 2010 and 2011, after correcting for foreground polarization through field star observation, reveal a decreasing level of polarization with wavelength, with the polarization angle independent of wavelength. However, reanalysis of literature data by applying our foreground correction method clarified the relative roles of electron scattering versus dust scattering in the circumstellar disk. Combining the multicolor data from the available epochs led us to conclude that a general electron scattering-dominated disk exists in both B[e] stars, with evidence of micron-sized grains seen at some epochs, likely condensed in the inner disk.

Key words: circumstellar matter – polarization – stars: emission-line, Be – stars: individual (HD 45677, HD 50138) – stars: variables: general

1. Introduction

The early-type objects show the characteristic permitted and forbidden line emission, known as B[e] stars, signifying rarefied gas in the envelopes. To explain their hybrid spectra, Zickgraf et al. (1985) used an empirical model with latitude-dependent winds, known as "two component model," consisting of a hot and fast radiative-driven wind in the polar region and a cool, dense wind along the dusty equatorial disk. Lamers et al. (1998) discussed the B[e] phenomenon for stars of various stellar evolutions, and in some known binaries with cool companions i.e., symbiotic stars; however, most B[e] objects have not been classified and are designated as unclassified B[e] stars, or unclB[e] stars. These B[e] stars likely remain unclassified because of their isolation from star-forming regions and lack of cold dust signature. Lee et al. (2016) conduct a thorough investigation of the interstellar and circumstellar environments surrounding eight unclB[e] stars. They concluded that these objects are not associated with any star-forming region. Moreover, no cold dust features are visible in their spectral energy distributions up to the millimeter wavelength. Therefore, in contrast to pre-main-sequence Herbig stars, which have rather similar observational properties, the dust grains surrounding B[e] stars are not derived from the natal molecular clouds but instead are formed in situ.

In the present study, we use multicolor polarimetry mainly in the optical range to investigate the properties of the in situ dust of isolated B[e] stars. Of the eight stars studied by Lee et al. (2016), HD 45677 and HD 50138 have convincing evidence for absence cold dust on the basis of millimeter measurements. Moreover, HD 45677 is the prototypical B[e] star (Swings 1977), and HD 50138 is the brightest known B[e] star.

Polarimetric imaging is a powerful tool for for studying circumstellar properties, including gas density and dust composition (Zickgraf & Schulte-Ladbeck 1989; Halonen & Jones 2013; Rivinius et al. 2013) and geometry (Magalhaes 1992; Melgarejo et al. 2001; Magalhães et al. 2006) in the inner disk, regardless of whether the disks or envelopes are resolved. B[e] stars exhibit intrinsic polarization (Magalhaes 1992) and are polarimetrically variable (Schulte-Ladbeck 1994; Oudmaijer & Drew 1999; Harrington & Kuhn 2009; Pereyra et al. 2009); however, their variability has not been sufficiently characterized.

Coyne & Vrba (1976) and Schulte-Ladbeck et al. (1992) reported a wavelength (λ) dependence in the polarization levels of HD 45677 observed during different epochs, signifying dust domination in the envelope. Oudmaijer & Drew (1999) studied its polarization in the Hα line region and determined that the continuum part of HD 45677 had changed between multiple observations, indicating that dust scattering is involved. However, for HD 50138, a contradictory conclusion was reached: it has a gas-dominated envelope, similar to classical Be stars (Bjorkman et al. 1998). Additionally, spectropolarimetric variation in the Hα line was reported by Oudmaijer & Drew (1999) but instead of the continuum part, its variability was mostly observed in the profiles of the double-peaked polarized line, indicating more than one line forming regions, which may interact. In addition to circumstellar composition, the disk geometry can also be estimated by polarization. HD 45677 and HD 50138 possess a similar disk position angle ($\sim$60°), derived using the polarization angle (Bjorkman et al. 1998; Patel et al. 2006). Their disk orientations were later confirmed through spatially resolved interferometry (Monnier et al. 2006; Borges Fernandes et al. 2009; Rodríguez et al. 2012; Ellerbroek et al. 2015; Kluska et al. 2016), along with the size of the inner gas disk component $\sim$50 mas for both targets (Monnier et al. 2009).

Because the observed polarization emerges as the intrinsic polarization convolved with interstellar polarization (ISP), we took special care in the ISP estimation. Before 2000, the ISP was hardly derived with field stars because of a lack of an archive stellar polarization and distance catalogs. However, we now have stellar polarization survey data from Heiles (2000)

and distance estimates from *Hipparcos* (van Leeuwen 2007) and *Gaia* (Gaia Collaboration et al. 2016), providing state-of-the-art data sets. By using the same ISP estimation from the same set of field stars, we can analyze our observation and reanalyze the literature data from different epochs, allowing us to conduct intrinsic and time resolved polarimetry for the first time.

This paper is structured as follows. In Section 2, we describe the data obtained from the literature and our own observations, as well as the data reduction procedures. In Section 3, we estimate the foreground polarization through field star observations, from which the intrinsic polarization of each of our targets is derived. In Section 4, we present the λ-dependence and its variability during different epochs. In Section 5, we discuss how the revised determination of intrinsic polarization delineates the role played by gas and dust in the envelopes of our targets.

2. Observations and Data Reduction

2.1. Literature Results and Our Observations

Several measurements of polarization have been carried out for HD 45677 by Coyne & Vrba (1976), Barbier & Swings (1982), Gnedin et al. (1992), and Schulte-Ladbeck et al. (1992) and for HD 50138 by Barbier & Swings (1982), Bjorkman et al. (1998), and Yudin & Evans (1998). Our observations of target, standard, and field stars were acquired on multiple nights, 2010 December 18, and 2011 November 5–7, using Aryabhatta Research Institute of Observational Sciences (ARIES) Imaging POLarimeter (AIMPOL; Rautela et al. 2004) mounted at the Cassegrain focus of the 104 cm Sampurnanand Telescope at ARIES, Nainital, India. AIMPOL comprises an achromatic half-wave plate (HWP) modulator, which measures the polarization state of the incoming light, and a Wollaston prism beam-splitter, which splits the light into two perpendicularly polarized beams. Field stars and our targets were observed through $BV(RI)_C$ polarimetry ($\lambda_B = 0.440\ \mu$m, $\lambda_V = 0.530\ \mu$m, $\lambda_{\rm Rc} = 0.670\ \mu$m, and $\lambda_{\rm Ic} = 0.800\ \mu$m) using a fraction ($370 \times 370$ pixels) of the TK (1024×1024 pixels) charge-coupled device (CCD) camera. Each pixel corresponds to 1.73 arcsec, and the field-of-view is approximately 8 arcmin in diameter. The full widths at half-maximum of the stellar images of the observations varied from 2 to 3 pixels. The readout noise and gain of the CCD are 7.0 e^{-1} and 11.98 e^{-1}/ADU, respectively.

Table 1
Measurements of Polarized Standard Stars

Band	$P \pm \epsilon_P$(%)	$\theta \pm \epsilon_\theta$(°)	$P \pm \epsilon_P$(%)	$\theta \pm \epsilon_\theta$(°)
	Our Work		Schmidt et al. (1992)	
2010 Dec 18				
	HD 25443			
B	5.22 ± 0.10	134.6 ± 0.5	5.23 ± 0.09	134.3 ± 0.5
V	5.31 ± 0.09	136.3 ± 0.5	5.13 ± 0.06	134.2 ± 0.3
R_c	4.81 ± 0.08	134.8 ± 0.4	4.73 ± 0.05	133.7 ± 0.3
I_c	4.30 ± 0.08	133.9 ± 0.5	4.25 ± 0.04	134.2 ± 0.3
	HD 19820			
B	4.92 ± 0.06	119.1 ± 0.4	4.70 ± 0.04	115.7 ± 0.2
V	4.80 ± 0.06	114.0 ± 0.3	4.79 ± 0.03	114.9 ± 0.2
R_c	4.53 ± 0.08	114.3 ± 0.5	4.53 ± 0.03	114.5 ± 0.2
I_c	4.06 ± 0.09	114.5 ± 0.6	4.08 ± 0.02	114.5 ± 0.2
2011 Nov 5				
	HD 7927			
B	2.76 ± 0.07	95.2 ± 0.7	3.23 ± 0.05	91.4 ± 0.4
V	3.06 ± 0.15	96.1 ± 1.4	3.30 ± 0.03	91.1 ± 0.2
R_c	3.17 ± 0.09	90.3 ± 0.8	3.03 ± 0.04	90.8 ± 0.3
I_c	2.77 ± 0.08	90.7 ± 0.8	2.78 ± 0.03	90.1 ± 0.3
	HD 19820			
B	4.59 ± 0.08	114.9 ± 0.5	4.70 ± 0.04	115.7 ± 0.2
V	4.63 ± 0.07	115.3 ± 0.5	4.79 ± 0.03	114.9 ± 0.2
R_c	4.62 ± 0.09	115.4 ± 0.5	4.53 ± 0.03	114.5 ± 0.2
I_c	4.18 ± 0.09	114.6 ± 0.6	4.08 ± 0.02	114.5 ± 0.2
2011 Nov 6				
	BD+59°389			
B	6.26 ± 0.10	98.1 ± 0.1	6.34 ± 0.04	98.1 ± 0.2
V	6.66 ± 0.09	98.2 ± 0.4	6.70 ± 0.01	98.1 ± 0.1
R_c	6.67 ± 0.06	97.8 ± 0.2	6.43 ± 0.02	98.1 ± 0.1
I_c	5.70 ± 0.06	97.5 ± 0.3	5.80 ± 0.02	98.3 ± 0.1
	HD 19820			
B	4.36 ± 0.07	115.9 ± 0.4	4.70 ± 0.04	115.7 ± 0.2
V	4.83 ± 0.05	115.2 ± 0.3	4.79 ± 0.03	114.9 ± 0.2
R_c	4.54 ± 0.07	115.0 ± 0.5	4.53 ± 0.03	114.5 ± 0.2
I_c	4.04 ± 0.08	114.5 ± 0.6	4.08 ± 0.02	114.5 ± 0.2
2011 Nov 7				
	HD 25443			
B	5.47 ± 0.09	134.9 ± 0.5	5.23 ± 0.09	134.3 ± 0.5
V	5.15 ± 0.10	133.5 ± 0.5	5.13 ± 0.06	134.2 ± 0.3
R_c	4.80 ± 0.11	137.0 ± 0.7	4.73 ± 0.05	133.7 ± 0.3
I_c	4.66 ± 0.09	131.9 ± 0.5	4.25 ± 0.04	134.2 ± 0.3

2.2. Data Reduction

The fluxes of the ordinary (I_o) and extraordinary (I_e) beams for all target, standard, and field stars were extracted by standard aperture photometry after bias subtraction using the IRAF[5] package. The ratio $R(\alpha)$ is given by

$$R(\alpha) = \frac{I_e(\alpha)/I_o(\alpha) - 1}{I_e(\alpha)/I_o(\alpha) + 1} = P\cos(2\theta - 4\alpha), \quad (1)$$

where P is the fraction of the total linearly polarized light, and θ is the angle of the plane of polarization. Here, α is the position of the fast axis of an HWP at 0°, 22.°5, 45°, or 67.°5, and the corresponding four normalized Stokes parameters are expressed as $q = (Q/I)$, $u = (U/I)$, $q1 = -(Q/I)$, and $u1 = -(U/I)$, respectively.

However, because the measured source intensities are imaged on a single frame, their ratio, I_e/I_o, should be corrected by using the following formula (Ramaprakash et al. 1998):

$$\frac{I_e(\alpha)}{I_o(\alpha)} = \frac{F_o}{F_e} \times \frac{I'_e(\alpha)}{I'_o(\alpha)} \quad (2)$$

where the ratio F_o/F_e is given as

$$\frac{F_o}{F_e} = \left[\frac{I'_o(0°)}{I'_e(45°)} \times \frac{I'_o(45°)}{I'_e(0°)} \times \frac{I'_o(22.°5)}{I'_e(67.°5)} \times \frac{I'_o(67.°5)}{I'_e(22.°5)}\right]^{\frac{1}{4}}. \quad (3)$$

This ratio can account for (a) the responsivity of the CCD to the two orthogonal polarization components and (b) the

[5] IRAF is distributed by National Optical Astronomical Observatories, USA.

Table 2
Polarization Values of HD 45677 and HD 50138 in 2010–2011

Date	P_B (%)	θ_B (°)	P_V (%)	θ_V (°)	P_{Rc} (%)	θ_{Rc} (°)	P_{Ic} (%)	θ_{Ic} (°)
				For HD 45677				
2010 Dec 18	1.11 ± 0.20	165.7 ± 5.4	1.30 ± 0.20	165.4 ± 4.4	0.85 ± 0.19	156.6 ± 6.3	0.74 ± 0.19	158.0 ± 7.3
2011 Nov 5	1.31 ± 0.19	161.8 ± 4.3	1.07 ± 0.19	160.6 ± 5.2	0.91 ± 0.19	158.6 ± 6.0	0.68 ± 0.19	164.5 ± 8.1
2011 Nov 7	1.29 ± 0.20	161.4 ± 4.5	1.13 ± 0.20	167.4 ± 5.1	1.02 ± 0.20	162.5 ± 5.6	0.75 ± 0.20	164.7 ± 7.8
				For HD 50138				
2010 Dec 18	0.82 ± 0.11	161.5 ± 3.6	0.71 ± 0.10	145.5 ± 4.2	0.71 ± 0.11	158.3 ± 4.6	0.51 ± 0.11	155.1 ± 6.0
2011 Nov 5	0.86 ± 0.11	142.8 ± 3.9	0.58 ± 0.12	160.9 ± 5.6	0.67 ± 0.12	151.8 ± 5.2	0.59 ± 0.12	157.7 ± 5.8
2011 Nov 6	0.84 ± 0.11	166.1 ± 3.7	0.42 ± 0.12	162.8 ± 7.9	0.63 ± 0.11	144.5 ± 5.3	0.54 ± 0.12	153.1 ± 6.5

responsivity of the CCD as a function of the positions on its surface. Therefore, if the correction is applied (Equation (3)) to the ratio I'_e/I'_o, a uniform response of the CCD would occur, which would replace the robust flat-fielding. By substituting Equations (2) and (3) into Equation (1) and fitting the cosine curve to the four values of $R(\alpha)$, the values of P and θ can be obtained.

Because the polarization accuracy is, in principle, limited by photon statistics, we estimated the errors in the normalized Stokes parameters $\sigma_{R(\alpha)}$ (σ_q, σ_u, σ_{q_1} and σ_{u_1} percentage) using

$$\sigma_{R(\alpha)} = \sqrt{(N_e + N_o + 2N_b)}/(N_e + N_o), \quad (4)$$

where N_e and N_o are the counts in the extraordinary and ordinary rays, respectively; N_b is the average background counts around the extraordinary and ordinary rays. The individual errors $\sigma_{R(\alpha)}$ associated with the four values of $R(\alpha)$ estimated using Equation (4) are used as weights when calculating P and θ for a particular target.

Because the polarization vectors are conventionally measured from the equatorial north and increase toward the east, the axis of the Wollaston prism is aligned with respect to the celestial north–south when the AIMPOL is mounted. Any offset is corrected by observing polarized standard stars. As shown in Table 1, the observed degree of polarization (in fraction; $P(\%)$) and polarization angle (degree θ) of the polarized standards in the $BV(RI)_C$ are in close agreement with those listed in Schmidt et al. (1992). According to several previous observations (Rautela et al. 2004; Medhi et al. 2007, 2008, 2010; Pandey et al. 2009; Eswaraiah et al. 2011), the AIMPOL has exhibited a stable instrument polarization of approximately 0.1% in $BV(RI)_C$ bands since 2004. Therefore, the instrumental contribution from the polarization level is considered stable. The observed multicolor polarization results for HD 45677 and HD 50138 and the observed dates are listed in Table 2. The results are corrected for offset polarization angles.

3. Data Analysis

3.1. Previous Foreground Estimates

Several studies have been attempted to estimate the ISP components of HD 45677 and HD 50138. Coyne & Vrba (1976) posited that the ISP of HD 45677 is the primary contributor to the observed polarization in the ultraviolet (UV) regime, because polarization at this wavelength is less variable than that in the red wavelengths. They posited the basis of the similarity between the observed length and orientation of the vectors connecting to the origin and the observed Stokes parameters (see their Figure 1) at multiple epochs. However, their assumption might be invalid, as discussed by Oudmaijer & Drew (1999). Another method is the depolarization of the Hα line-center, because emitted line photons are commonly assumed to be unpolarized. However, this method can only derive part of the intrinsic polarization (because of electron scattering) caused by the circumstellar gas alone ($P = 0.87\%$ at $\theta = 75°$, Patel et al. 2006).

The ISP of HD 50138 was estimated by Bjorkman et al. (1998) as $P = 0.2\%$ at $\theta = 170°$. These values represent the mean of ISPs from three methods. (1) Only three field stars can be used for ISP calibration, but more field stars are necessary to serve as a representative ISP contribution. (2) The polarization changes across the Hα line. Because of a considerable change in Hα line, as reported by Oudmaijer & Drew (1999) and Harrington & Kuhn (2009), this method is inapplicable. (3) The ISP component of HD 45677 estimated by Coyne & Vrba (1976) was adopted. As already stated, the ISP estimate for HD 45677 from the literature is unreliable.

Therefore, our goal is to reanalyze the multiepoch polarization data reported in the literature and to contribute our own observations through improved and reliable ISP correction to derive the intrinsic polarizations of our targets.

3.2. Our Foreground Estimation

Because of the small projected angular separation of approximately 8° (R.A. = $6^h39^m55^s.42$, decl. = $-10°0'35''.28$) of the sky and line-of-sight distance between HD 45677 (601 ± 123 pc) and HD 50138 (340 ± 47 pc), we first collected the field stars around both targets and subsequently decided on a proper field region. Within a 10° radius of both B[e] stars, we selected 42 field stars from either archived polarization data cataloged by Heiles (2000) or among those we observed using the AIMPOL. The field stars distances were taken from Hipparchus catalog (van Leeuwen 2007) and the newly available *Gaia* catalog (Gaia Collaboration et al. 2016). Stars flagged for variability, emission, or double stars were excluded using the SIMBAD Astronomical Database. Table 3 lists the adopted polarization data for all of the field stars along with their HD numbers, spectral types, distances, and the radial distances from our targets. Among all the field stars with AIMPOL data, HD 43068 and HD 44892 also have archive results (Heiles 2000), which are $P_V = 0.37\% \pm 0.06\%$, $\theta_V = 57° \pm 5°$ and $P_V = 0.57\% \pm 0.05\%$, $\theta_V = 95° \pm 3°$, respectively; their AIMPOL measurements are $P_V = 0.56\% \pm 0.07\%$, $\theta_V = 50° \pm 4°$, $P_V = 0.61\% \pm 0.09\%$, $\theta_V = 87° \pm 4°$. The archived results and our measurements are generally consistent for these two field stars, indicating the favorable performance of AIMPOL.

Table 3
Polarization Measurements, HD Numbers, Distances (from *Hipparcos* or *Gaia* Catalog), and Radial Distances of 42 Field Stars Distributed within the 10° Radius Fields of HD 45677 and HD 50138

No.	Field Star	Spectral Type	Distance (pc)	P_V (%)	θ_V	Angular to HD 45677	Angular to HD 50138
1	HD 40088	A1III/IV	503 ± 68[a]	0.76 ± 0.13	55 ± 5	9.°0	13.°8
2	HD 40118	A0V	495 ± 81[a]	0.26 ± 0.05	50 ± 5	9.°5	13.°6
3	HD 40728	B8V	289 ± 31[a]	0.15 ± 0.03	45 ± 5	8.°8	12.°7
4	HD 40878	B8III	1010 ± 255[a]	0.26 ± 0.05	21 ± 5	8.°5	12.°5
5	HD 40986	B9V	544 ± 109[a]	0.62 ± 0.11	65 ± 5	9.°0	12.°3
6	HD 40761	B9IV	769 ± 225[a]	1.30 ± 0.22	45 ± 5	7.°5	12.°9
7	HD 41207[b]	A0III/IV	429 ± 48[a]	2.04 ± 0.35	40 ± 5	8.°1	12.°0
8	HD 42051	B2II	885 ± 196[a]	1.75 ± 0.20	104 ± 3	8.°1	10.°7
9	HD 42690	B2II	366 ± 36[c]	0.15 ± 0.00	53 ± 0	7.°7	9.°9
10	HD 42712	F2V	164 ± 7[a]	0.12 ± 0.07	50 ± 16	4.°0	11.°6
11	HD 42947	F0V	276 ± 24[a]	0.50 ± 0.09	63 ± 5	4.°3	12.°5
12	HD 42965[d]	K0II/III	538 ± 93[a]	0.63 ± 0.18	71 ± 9	4.°4	12.°7
13	HD 43068[d]	A9V	238 ± 48[c]	0.56 ± 0.07	50 ± 4	4.°3	12.°6
14	HD 43028[d]	G8III	175 ± 12[a]	0.29 ± 0.09	50 ± 4	4.°3	12.°6
15	HD 43543	A9V	222 ± 12[a]	0.14 ± 0.01	46 ± 3	4.°4	12.°7
16	HD 43781	A7/8IV/V	246 ± 16[a]	0.10 ± 0.05	30 ± 13	4.°7	13.°1
17	HD 44340	F2V	170 ± 10[a]	0.21 ± 0.03	44 ± 4	2.°0	10.°2
18	HD 44440	F0V	343 ± 35[a]	0.46 ± 0.07	66 ± 4	3.°1	11.°4
19	HD 44588	A9V	375 ± 37[a]	0.46 ± 0.06	48 ± 4	1.°6	9.°8
20	HD 44756	A0V	120 ± 5[a]	0.10 ± 0.04	173 ± 10	8.°5	7.°4
21	HD 44800	A8IV	100 ± 4[a]	0.01 ± 0.01	120 ± 18	2.°2	10.°5
22	HD 44892[b d]	A9/FOIV	188 ± 14[a]	0.61 ± 0.09	87 ± 4.3	3.°6	11.°7
23	HD 45032	F2V	324 ± 30[a]	0.28 ± 0.10	79 ± 10	3.°8	11.°9
24	HD 45433	K2/3III	212 ± 17[c]	0.10 ± 0.04	27 ± 10	12.°8	9.°0
25	HD 45629[d]	B9III	189 ± 18[a]	0.21 ± 0.05	51 ± 7	7.′9	8.°5
26	HD 45733[d]	A2	100 ± 4[a]	0.17 ± 0.06	54 ± 11	4.′2	8.°3
27	HD 46064	B2III	398 ± 119[a]	0.45 ± 0.10	67 ± 1	0.°6	8.°1
28	HD 46185	B2/3(II)	380 ± 80[c]	0.25 ± 0.03	51 ± 3	0.°9	7.°5
29	HD 46229	K2III	214 ± 12[c]	0.23 ± 0.04	160 ± 4	5.°0	5.°0
30	HD 46487	B5IV/V	170 ± 7[c]	0.19 ± 0.10	68 ± 1	11.°9	7.°3
31	HD 46769[b]	B7Ib-II	467 ± 85[c]	1.06 ± 0.2	124 ± 5	14.°1	8.°8
32	HD 48867	A8III	307 ± 29[a]	0.39 ± 0.07	79 ± 5	13.°3	6.°7
33	HD 48933	A3IV/V	258 ± 18[a]	0.33 ± 0.04	79 ± 3	12.°6	5.°9
34	HD 49315[b]	B4III	483 ± 110[a]	0.78 ± 0.04	25 ± 2	5.°5	9.°2
35	HD 49741[d]	K2/3III	340 ± 37[a]	0.16 ± 0.09	24 ± 16	7.°7	40.′0
36	HD 50252[d]	B9V	246 ± 19[a]	0.17 ± 0.07	68 ± 12	8.°8	31.′6
37	HD 50529	A5IV/V	461 ± 68[a]	0.30 ± 0.02	74 ± 2	15.°2	7.°7
38	HD 51148	F0V	190 ± 11[a]	0.13 ± 0.06	91 ± 14	13.°9	6.°1
39	HD 54439	B2/3II	827 ± 383[a]	0.83 ± 0.18	136 ± 6	9.°9	6.°4
40	HD 55185	A0IV	118 ± 2[c]	0.10 ± 0.01	41 ± 2	16.°6	8.°2
41	HD 55879	O9III	870 ± 287[c]	0.51 ± 0.20	142 ± 11	11.°6	6.°6
42	HD 57682	O9IV	752 ± 334[a]	0.37 ± 0.2	180 ± 15	13.°8	7.°8

Notes. Spectral types were obtained from SIMBAD.
[a] Gaia Collaboration et al. (2016).
[b] Stars with scattered distribution of Stokes parameters. These were not used while performing the weighted linear fits and estimating the ISP values (see Figure 2).
[c] van Leeuwen (2007).
[d] Measurements with AIMPOL.

Table 4
ISP Contributions of Stokes Parameters and Polarization Level and Angle for HD 45677 and HD 50138

Name	Distance (pc)	Q_{ISP} (%)	U_{ISP} (%)	P (%)	θ (°)
HD 45677	601 ± 123	−0.46 ± 0.17	0.68 ± 0.21	0.82 ± 0.19	62 ± 6
HD 50138	340 ± 47	−0.22 ± 0.10	0.13 ± 0.06	0.26 ± 0.10	74 ± 9

For HD 43068 and HD 44892, we used the AIMPOL results instead of the archive.

With the polarization of these 42 field stars, we first constrain a linear range of this ISP component by checking the polarization distribution along the distance. As shown in the Figure 1(a), the P_V values exhibit an increasing trend as a function of distance up to ∼733 pc, whereas θ_V as shown in Figure 1(b) has value, mostly distributed between 20° and 100°, up to a distance of 733 pc. Beyond which, both P_V and θ_V exhibited an abrupt change. Notably, Lee et al. (2016) reported

Table 5
$P_{\rm int}$ and $\theta_{\rm int}$ of HD 45677 and HD 50138

Date	P_B (%)	θ_B (°)	P_V (%)	θ_V (°)	$P_{\rm Rc}$ (%)	$\theta_{\rm Rc}$ (°)	$P_{\rm Ic}$ (%)	$\theta_{\rm Ic}$ (°)
				For HD 45677				
2010 Dec 18	1.08 ± 0.20	166.7 ± 4.7	1.21 ± 0.16	167.1 ± 3.7	0.78 ± 0.15	157.7 ± 5.4	0.67 ± 0.14	159.5 ± 6.1
2011 Nov 5	1.28 ± 0.17	162.6 ± 3.7	0.97 ± 0.15	162.3 ± 4.5	0.85 ± 0.15	159.8 ± 5.2	0.62 ± 0.15	166.8 ± 7.0
2011 Nov 7	1.26 ± 0.18	162.2 ± 4.0	1.05 ± 0.16	169.5 ± 4.3	0.96 ± 0.16	163.8 ± 4.8	0.69 ± 0.16	166.8 ± 6.7
				For HD 50138				
2010 Dec 18	0.89 ± 0.09	157.4 ± 2.9	0.82 ± 0.09	142.6 ± 2.6	0.79 ± 0.10	153.9 ± 3.7	0.59 ± 0.09	150.4 ± 4.1
2011 Nov 5	0.99 ± 0.10	141.1 ± 2.9	0.64 ± 0.10	155.3 ± 4.3	0.76 ± 0.11	148.0 ± 4.0	0.66 ± 0.10	153.2 ± 4.4
2010 Nov 6	0.89 ± 0.10	161.7 ± 3.1	0.47 ± 0.10	155.0 ± 6.1	0.75 ± 0.10	141.6 ± 3.8	0.63 ± 0.10	148.8 ± 4.7

that two known star-forming regions, Mon-R2 (800 pc) and CMa OB1 (1150 pc), are located just beyond 733 pc and distributed within 10° field of HD 45677/HD 50138. Therefore, we exclude these distant field stars from further analysis because they may not represent the true ISP values to our targets.

After establishing a distance limit for the ISP component, here we choose the proper field stars over an angular area projected on the sky around HD 45677 and HD 50138 by plotting their polarization vector map (Figure 2). Within 340 pc, the polarization angles of the field stars in the vicinity of each target have slightly different orientations, indicating that the ISP components for the two line of sights to our targets cannot be considered the same. Furthermore, as illustrated in the Appendix, we notice that unreliable ISP components may result if we use the field stars of either (a) individual 10° fields around each target, or (b) common 10° field enclosing both targets. Therefore, to avoid this, we estimate more reliable ISP components using the independent populations of field stars of the respective target that are separated by a sharp boundary shown with a green line in Figure 2. Additional details on our ISP estimations using different field stars selections are given in the Appendix.

With the selection range of the field regions, we estimated the independent ISP values for HD 45677 and HD 50138 using the following steps. First, we convert P_V and θ_V of the field stars around individual B[e] stars into Stokes parameters using the relations $Q_V = P_V \cos(2\theta_V)$ and $U_V = P_V \sin(2\theta_V)$. Second, we perform weighted linear fits on the distance versus Stokes parameters as shown in the Figure 3. Fitted slopes and intercepts are used to estimate the resultant ISP Stokes parameters ($Q_{\rm ISP}$ and $U_{\rm ISP}$) at the given distances of our two targets. When performing the weighted linear fits, we exclude several stars exhibiting a scattered distribution of Stokes parameters (marked as overlapping open circles) in addition to the stars with distances of >733 pc. Third, derived $Q_{\rm ISP}$ and $U_{\rm ISP}$ values at the distances of the B[e] stars are converted back to the $P_{\rm ISP}$ and $\theta_{\rm ISP}$ values and presented in Table 4 along with their propagated uncertainties.

3.3. Intrinsic Polarization

With the ISP in terms of $Q_{\rm ISP}$ and $U_{\rm ISP}$, we can estimate the intrinsic polarization ($P_{\rm int}$ and $\theta_{\rm int}$) of HD 45677 and HD 50138. The intrinsic Stokes parameters $Q_{\rm int}$ and $U_{\rm int}$ are given by

$$Q_{\rm int} = Q_\star - \langle Q_{\rm ISP} \rangle \quad (5)$$

and

$$U_{\rm int} = U_\star - \langle U_{\rm ISP} \rangle, \quad (6)$$

where $Q_\star$ and $U_\star$ are the Stokes parameters derived from the observed polarization of HD 45677 and HD 50138. Subsequently, $Q_{\rm int}$ and $U_{\rm int}$ are converted into $P_{\rm int}$ and $\theta_{\rm int}$.

In addition to the derived ISP contribution at the V band, we estimate the ISP contribution at other wavelengths. This enables us to extract the ISP contributions from the observed literature-based data. By using the Serkowski's law (Serkowski et al. 1975), that is, $P_v = P_{\rm max} \exp[-K\, ln^2(\lambda_{\rm max}/\lambda)]$, where $P_{\rm max}$ is the peak polarization, occurring at wavelength $\lambda_{\rm max}$. We assume that $\lambda_{\rm max} = 0.55$ μm so that $P_{\rm max} = P_V = 0.24\%$. Adopting $K = 1.66\ \lambda_{\rm max} + 0.01$ (Whittet et al. 1992), we derive an average ISP as a function of wavelength. Table 5 lists our measured intrinsic polarization values of HD 45677 and HD 50138 for different epochs in $BV(RI)_C$.

3.4. Reanalysis of Previous Observations

Herein, we present the reanalysis of literature data, including those of Coyne & Vrba (1976) and Schulte-Ladbeck et al. (1992) for HD 45677 and Bjorkman et al. (1998) for HD 50138, by applying our ISP corrections. Their originally derived intrinsic polarization is also presented for comparison. Figure 4 presents $P_{\rm int}$ and $\theta_{\rm int}$ of HD 45677 measured from 1971 to 1975 by Coyne & Vrba (1976) from optical to near-infrared wavelengths. Almost all the original results exhibit an increasing trend longward of 0.5 μm. Large dust grains ($\gtrsim$1 μm) were suggested as the main scatterers of starlight. By contrast, we estimated a completely different λ dependence. At shorter wavelengths (0.35–0.5 μm), our revised $P_{\rm int}$ values are higher than the original literature; at longer wavelengths ($\gtrsim$0.5 μm), our results are lower. Regarding $\theta_{\rm int}$, our revised results from four different epochs all show a λ independence shortward of 0.7 μm, justifying the ISP correction's reliability. Notably, the one data point at 0.6 μm is not an outlier anymore after reanalysis of previous observations.

Also for HD 45677, Figure 5 presents $P_{\rm int}$ and $\theta_{\rm int}$ on the basis of the spectropolarimetric data provided by Schulte-Ladbeck et al. (1992) covering the range 0.1–0.75 μm. Longward of 0.35 μm, the λ-dependence of the polarization corresponds to the results of Coyne & Vrba (1976), probably because the same ISP was adopted. Shortward of 0.25 μm, the polarization exhibits an increase toward shorter wavelengths. A polarization angle flip of 90° occurs at 0.2–0.3 μm, which Schulte-Ladbeck et al. (1992) suggested as evidence of a thick dust disk and a thin dusty bipolar region. With our revised ISP, the updated λ dependence of $P_{\rm int}$ of the 1990 data differs

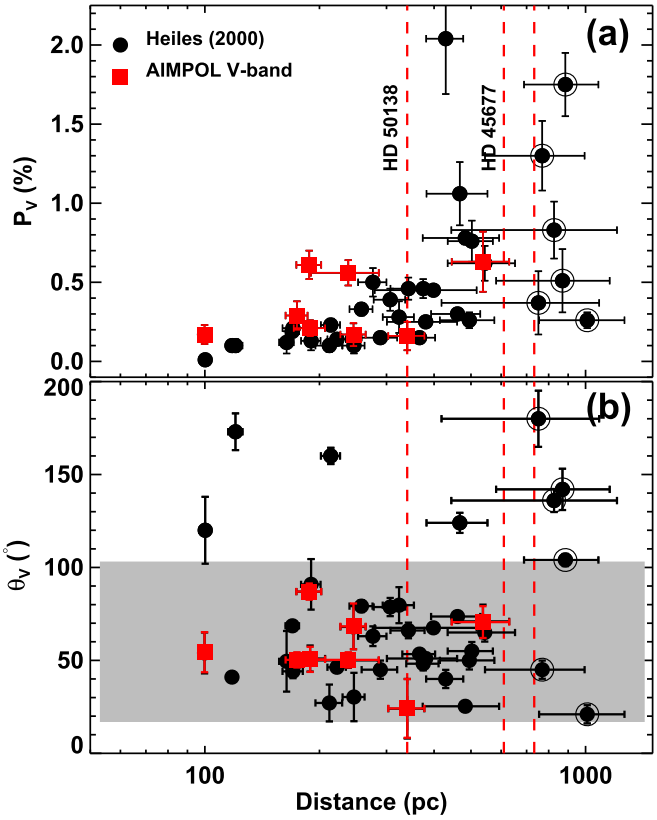

Figure 1. P_V (a) and θ_V (b) vs. distance plots for the 42 field stars. Of these, 34 field stars with Heiles polarization data (filled circles) and 8 field stars with AIMPOL data (filled red squares). Red dashed lines are drawn at the distances of 340 pc (HD 50138), 610 pc (HD 45677), and 733 pc (distance + $1\sigma_{\rm distance}$ of HD 45677). The P_V values increase steadily with distance up to approximately 733 pc, and the θ_V values are mostly distributed between 20° and 100° (illustrated with gray shaded background). Stars with distances of >733 pc, shown encircled, exhibit an abrupt change both in P_V and θ_V.

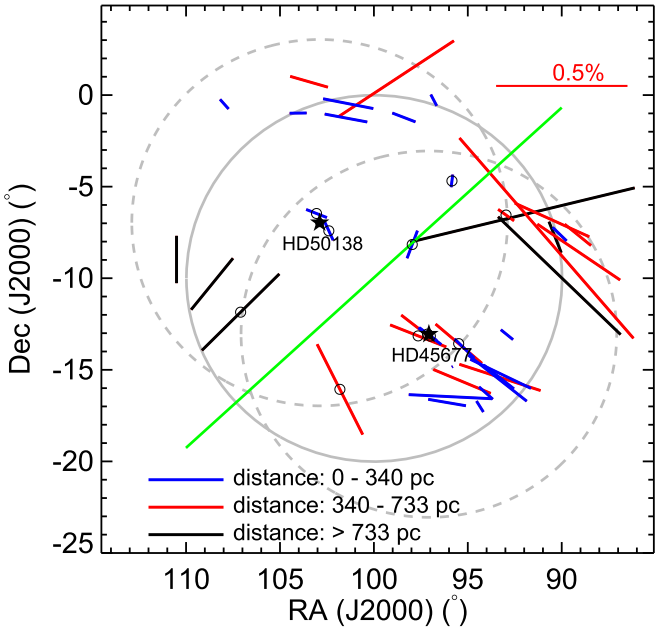

Figure 2. Vector map using polarization measurements of 42 field stars located toward the region containing both B[e] stars HD 50138 and HD 45677. The locations of these two B[e] stars are marked using star symbols. The dashed gray circles denote the 10° radii fields around HD 50138 and HD 45677, whereas the solid gray circle denotes the 10° radius field around the middle point of HD 50138 and HD 45677. Polarizations of field stars with distances of <340 pc, 340 pc–733 pc, and >733 pc are shown with blue, red, and black colored vectors, respectively. Stars distributed within the overlapping area of two dashed circles are denoted using open circles. The green line passing through the mid point of HD 50138 and HD 45677 separates the field stars with different polarization characteristics. Additional details on the region selection used for ISP estimation are presented in the Appendix.

greatly at optical wavelengths, with $\theta_{\rm int}$ increasing gradually with wavelength from 150° to 30° with no sudden flip.

The reanalysis results of HD 50138 are presented in Figure 6. Its spectropolarimetric data, recorded in 1995 and presented by Bjorkman et al. (1998), yield an almost λ-independent polarization from UV to optical wavelengths, suggesting Thomson scattering in a geometrically thin disk at a high inclination angle, as often observed in classical Be stars. Although the revised $P_{\rm int}$ (∼1.0%) had a similar λ-dependence, the polarization level is systematically higher than the original value (∼0.5%) in the optical wavelengths. We further discuss this change in Section 5.

Notably, the new derived $P_{\rm int}$ and $\theta_{\rm int}$ values of both HD 45677 and HD 50138 are close to their observed values, revealing the minor role of foreground polarization from this line of sight up to the distances of our targets. Therefore, we can evaluate the intrinsic polarization as reported in the literature during early epochs at long wavelengths (e.g., in the infrared, for which we did not have field star observations).

4. Wavelength Dependence and Variability

In this section, we incorporate the results derived from the literature, those with measurements from at least three bands, and our own observations to investigate the temporal and possible in situ dust formation, on the basis of the λ dependence and variability of P_λ and θ_λ.

For HD 45677, we plot the results from different epochs, including 11 sets of multiband measurements, as shown in Figure 7. In the 2010s, the three sets of data with separations of 1 year and 1 day exhibit similar behavior, with a gradually decreasing trend of P_λ toward longer wavelengths. This tendency can also be seen for all eight other sets of literature data after our ISP removal. These modified results from the literature include some measurements from beyond the optical wavelength, including UV and near-infrared. In all historic epochs, $P_{\rm int}$ in the U band is significantly smaller than in the B band; thus, the maximum P_λ is likely to be approximately 0.45 μm. By contrast, the minimums can be seen in the 1990s at 0.8–0.9 μm. For θ_λ, λ-independence is most shown, especially in our measurement of 2010–2011. Other epochs also exhibit general θ_λ independencies limited within 0.3 μm to 0.5–0.6 μm. In contrast to the case at short wavelengths, P_λ greater than approximately 0.5 μm varied significantly with time. An occasional rise up from 150° to 70° was observed, i.e., a nearly 90° difference, comparable to "wagging tail" behavior with turning points at different wavelengths.

For HD 50138 in the optical wavelength, as presented in Figure 8, three data sets of current observation exhibit λ dependence with a consistently decreasing $P_{\rm int}$ toward long wavelengths, with a noticeable variation in the V band. A similar decreasing trend was seen in 1980. The three measurements obtained in 1995, including one spectropolarimetry measurement for an optical wavelengths of up to 0.9 μm, are all λ independent. In the UV region, however, these data from the literature show substantial variability; some observations conducted within only two months. By contrast, $\theta_{\rm int}$ of

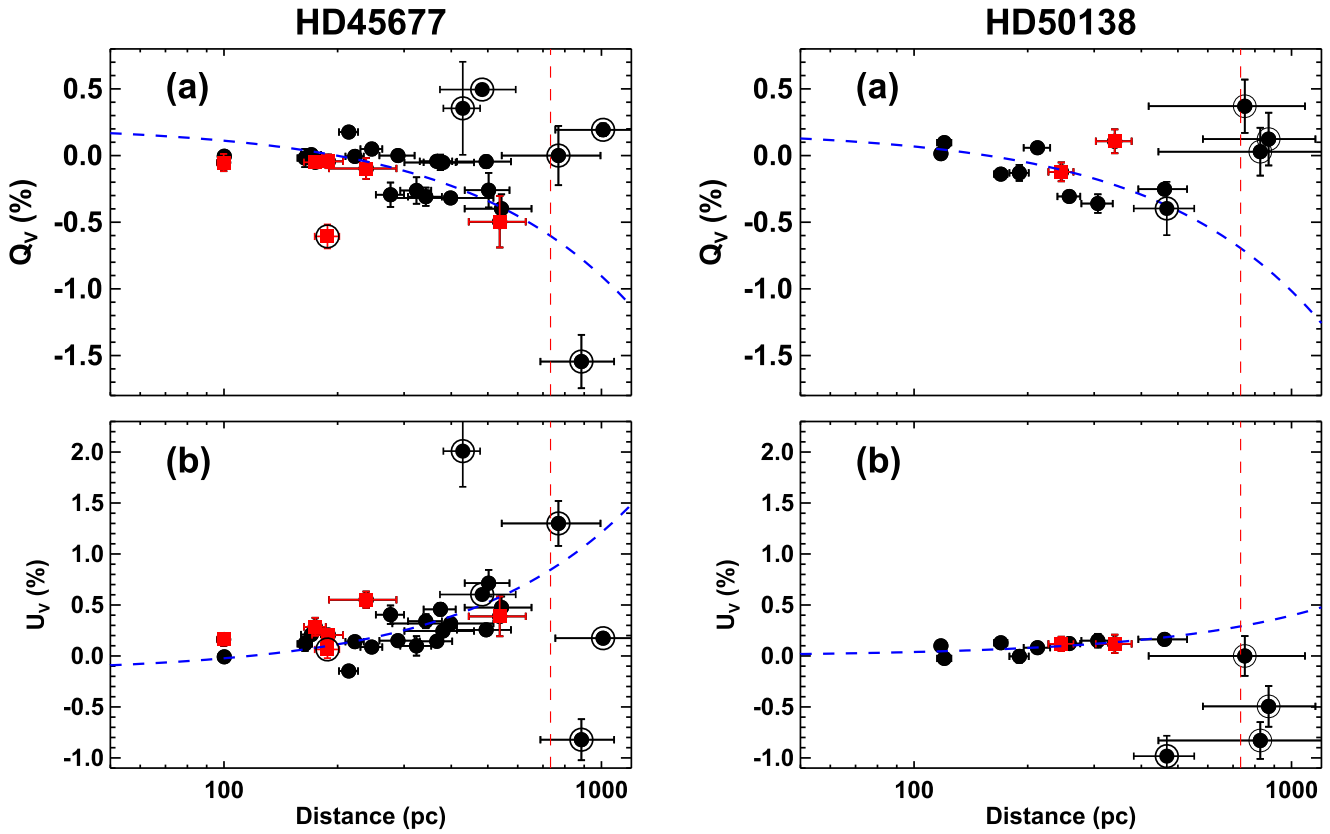

Figure 3. Stokes parameters vs. distance plots for deriving the ISP values at the distances of the B[e] stars. (a) Q_V vs. distance and (b) U_V vs. distance plots for 28 field stars (22 from Heiles (2000) and 6 from AIMPOL data) distributed around HD 45677 but that fall below the green line in Figure 2. (c) Q_V vs. distance and (d) U_V vs. distance plots of 14 field stars (12 from Heiles (2000) and 2 from AIMPOL data) distributed around HD 50138 but that fall above the green line in Figure 2. In each panel, the weighted linear fits on the Stokes parameters vs. distances are shown using blue dashed lines. Notably, stars with distances $>$ 733 pc and with scattered distribution of Stokes parameters, shown encircled, were not used in the fits.

HD 50138 is likely to be λ independent for all epochs, remaining in a relatively narrow range from 140° to 170°.

5. Discussion

The strong infrared excess of B[e] stars is evidence for dust existing in their circumstellar disk (Allen 1973; Lee et al. 2016). However, the dust feature is partially observed by polarimetry. Magalhães et al. (2006) determined that the polarization characteristics of B[e] supergiants in the Magellanic Clouds are most likely dominated by electron scattering instead of dust scattering, (e.g., HD 34664 and S111, Schulte-Ladbeck & Clayton 1993; Melgarejo et al. 2001). Even among the galactic B[e] stars studied by Zickgraf & Schulte-Ladbeck (1989), half of the sample are dust dominated. Among B[e] stars with significant intrinsic polarization, the main polarizing mechanisms are electron scattering for MWC 645 and MWC 939 and dust scattering for MWC 623 and MWC 342.

Both of our two targets have prominent near-infrared excess similar to other B[e] stars and the spectral energy distributions falling beyond the mid-infrared wavelengths, yet with relatively low foreground extinction, indicating the existence of hot and warm dust with a nonspherical spatial distribution and lack of cold grains in the outer envelopes (Lee et al. 2016). In our polarization data, HD 45677 and HD 50138 exhibit gas-dominated signatures in most epochs, in common with other B[e] stars. Despite electron scattering, dust scattering can be seen in some epochs from the data sets covering several decades.

Electron scattering is characterized by either a flat or a sawtooth-like P_λ dependence, which is commonly seen among classical Be stars (Coyne & Kruszewski 1969; Wood et al. 1997). The flat pattern is attributable to the scattering of low-density electrons. Once the scattered light is attenuated by bound-free opacities in a dense disk, abrupt changes in the polarization patterns occur at the hydrogen series limits, such as Balmer or Paschen, resulting in a sawtooth pattern manifesting as a wavy P_λ in broad-band measurements. One such P_λ pattern can therefore be used as a measure of the density of the circumstellar disk of known Be stars (Halonen & Jones 2013).

Wisniewski et al. (2007) used this P_λ pattern to authenticate a classical Be star candidate. Stars with highly classical Be characterization are classified as type 1. For all available epochs, the P_λ of HD 45677 is very close to type 1. HD 50138 also shows a type-1-like phase in 1980 and in our 2010 and 2011 measurements despite its 1995 results. Poeckert et al. (1979) investigated the polarization nature of 70 classical Be stars using the quantity $(P_{4060} - P_{7800})/P_{4060}$ across the Paschen continuum. They determined those with polarization $P_{4060} > 1\%$ had prominent Paschen slopes of 0.0–0.6, and stars with shell spectra or strong hydrogen emission, suggesting a high density along the line of sight, tended to exhibit higher values. Our targets also belong to the class called shell stars (Merrill 1949; Borges Fernandes et al. 2009). In our measurements, the slopes of the Paschen continuum are approximately 0.6 for HD 45677, and 0.5 for HD 50138, which are near the upper end of empirical values for shell stars,

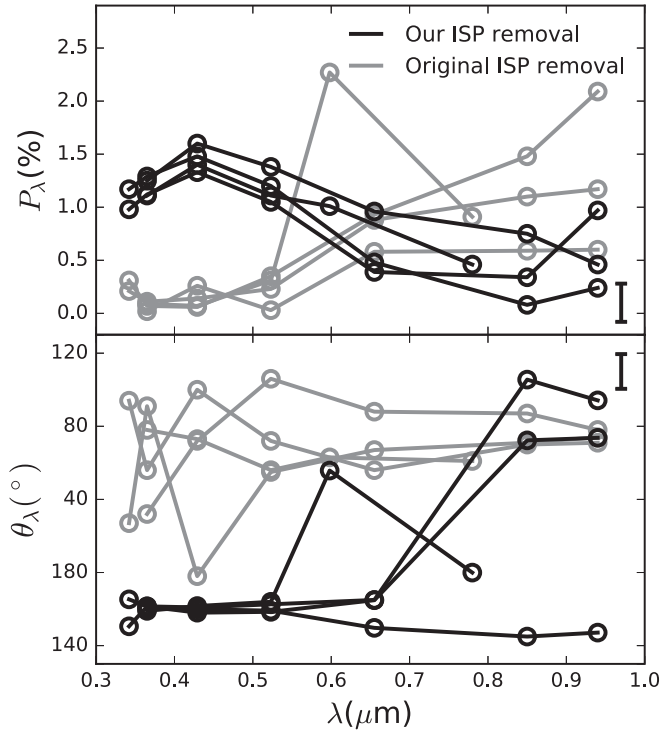

Figure 4. Intrinsic polarization $P_{\rm int}$ and $\theta_{\rm int}$ of HD 45677. The gray lines indicate the original intrinsic polarization given by Coyne & Vrba (1976), whereas the black lines represent the intrinsic polarization derived with the revised ISP correction (from this work).

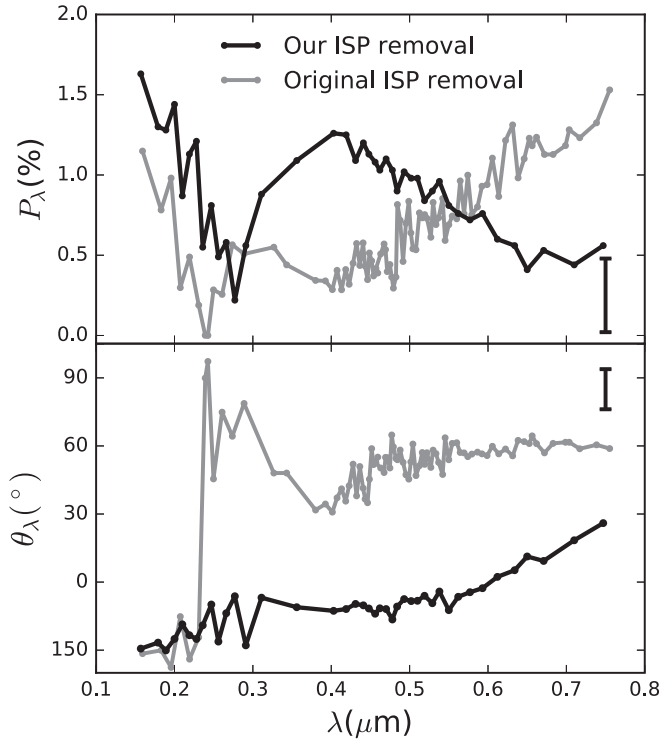

Figure 5. Intrinsic polarization, $P_{\rm int}$ and $\theta_{\rm int}$, of HD 45677. The gray line indicates the original intrinsic polarization published by Schulte-Ladbeck et al. (1992). The black line represents the intrinsic polarization derived with the revised ISP correction (from this work).

indicating domination of the gas with high opacity. This sawtooth-like P_λ is not the only common feature between our targets and classical Be stars. In terms of their optical and

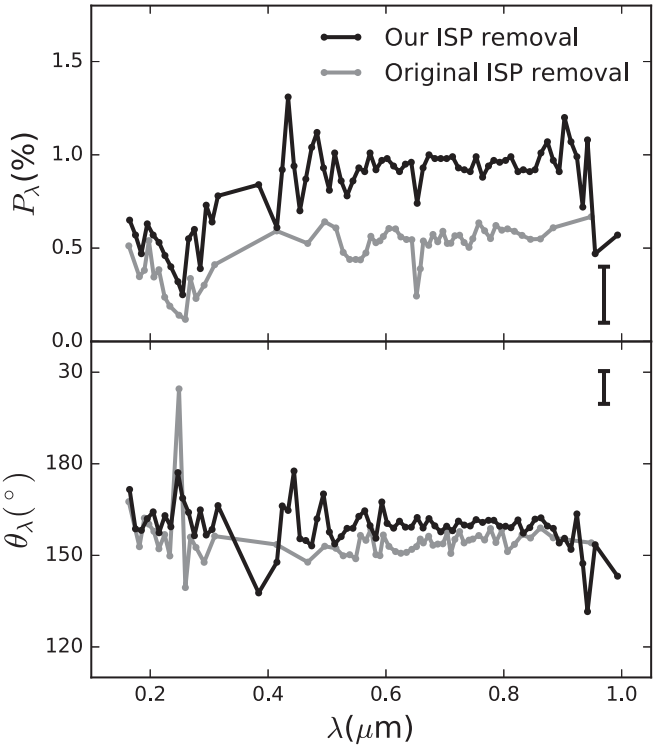

Figure 6. Intrinsic polarization, $P_{\rm int}$ and $\theta_{\rm int}$, of HD 50138. The gray line depicts the result reported by Bjorkman et al. (1998). The black line presents our revised result.

near-infrared spectroscopic characteristics, Lamers et al. (1998) indicated that these two B[e] stars have the potential to be "main sequence B[e] stars" or "extreme classical Be stars."

Although polarization level varied from epoch to epoch, the general sawtooth-like pattern of HD 45677 has lasted for several decades since 1970s, exhibiting similar λ dependence from the UV to optical wavelength. The rising P_λ longward of the I band can be observed in some epochs before 1990, possibly attributable to micrometer-sized dust grains. We suggest that abundant dust condensation occurs because of copious stellar wind, as seen in HD 45677, for which the level of infrared excess exceeds the stellar photospheric radiation. For θ_λ, most measurements show a position angle of approximately 160° in optical wavelengths, consistent with that reported by Oudmaijer & Drew (1999) and Patel et al. (2006). This implies a perpendicular scattering envelope, as evidenced by the interferometric results of elongation at approximately 70° in the near- to mid-infrared (Monnier et al. 2006, 2009) and at approximately 90° in the millimeter wavelengths (Rodríguez et al. 2012). By contrast, before 1990, a rotating θ toward longer wavelength could be seen in many epochs, indicative of ejection with gas and newly formed dust with different elongations from the main disk.

For HD 50138, a similar electron scattering signature could be observed in 1980 and 1995, exhibiting a Balmer jump at 0.4 μm. In the optical wavelength, however, $P(\lambda)$ exhibits λ-independence up to 0.9 μm, likely due to a superposition of gas and dust grains with a wide range of size distribution (approximately 0.5–0.9 μm). Instead of the minor contributions suggested by Bjorkman et al. (1998), the dust component contributed significantly to λ-dependence of polarization, after ISP correction. Moreover, some days earlier in 1995, two measurements exhibited U band polarization clearly higher

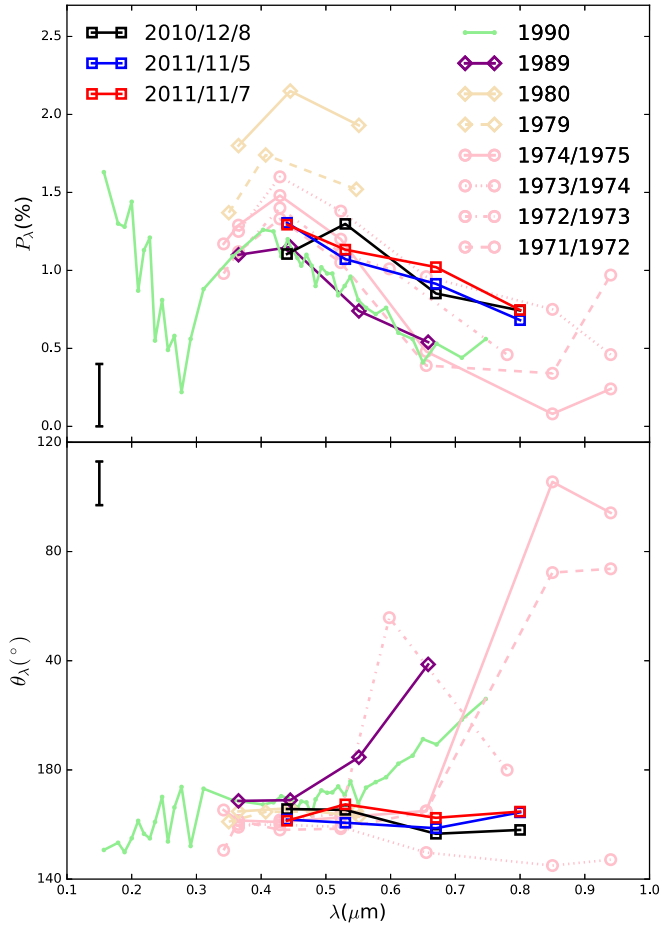

Figure 7. Intrinsic P_λ and θ_λ for different epochs of HD 45677, as indicated in the legend. Two representative error bars for P (bottom left) and θ (upper left) are presented. Squares connected by black, blue, and red lines correspond to our observations, along with other data from the literature after correction with our ISP, including Schulte-Ladbeck et al. (1992, light green), Gnedin et al. (1992, purple), Barbier & Swings (1982, wheat), and Coyne & Vrba (1976, pink).

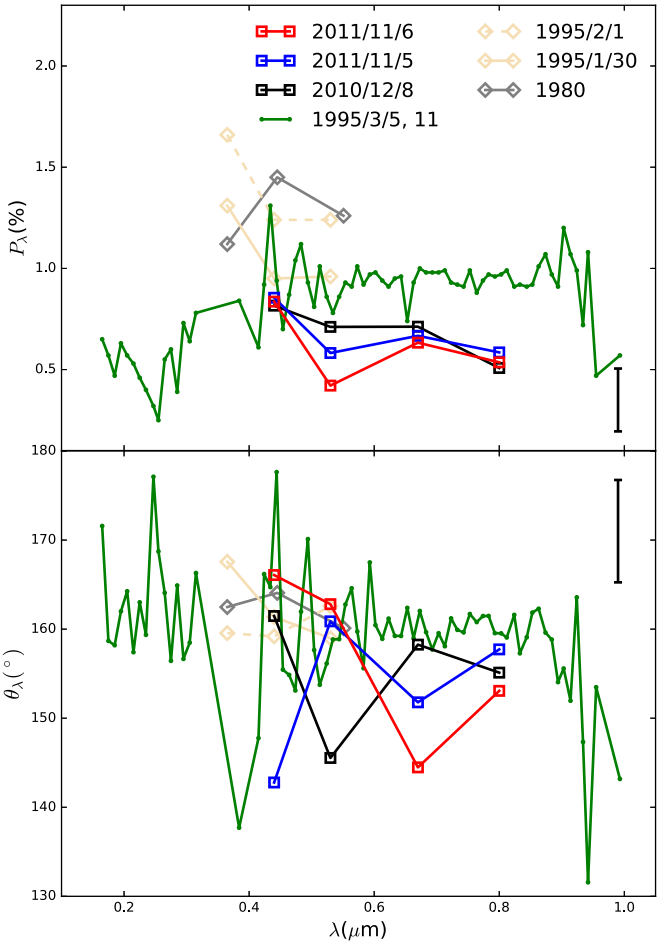

Figure 8. Intrinsic P_λ and θ_λ for different epochs of HD 50138, as indicated in the legend. Two representative error bars for P (bottom right) and θ (upper righ) are presented. Squares connected by red, blue, and black lines correspond to our observations, along with other data from the literature after correction with our ISP, including Bjorkman et al. (1998, green), Yudin & Evans (1998, wheat), and Barbier & Swings (1982, gray).

than that of the BV band. This polarization distribution over λ is likely attributable to the formation of small grains in the inner edge of the disk. These grains increased in size within a very short timescale. For θ_λ, HD 50138 has an intrinsic polarization angle of approximately 155° in the optical wavelengths. Interferometry yielded an elongation of approximately ∼70° in the near-infrared wavelengths (Borges Fernandes et al. 2011; Kluska et al. 2016).

As discussed, polarization resulting from dust scattering was occasionally detected. In the inner part of the disk, we are likely to witness the in situ dust formation proposed by Lee et al. (2016). The size of a dust grain can be in submicron scale in HD 50138, or more than 1 micron such as in HD 45677, suggesting a rapid grain growth rate. In contrast to B[e] supergiant polarization, which can be explained by electron scattering (Magalhães et al. 2006), our targets may be on the verge of turning-off main sequence; thus, the dust can be formed sufficiently close to scatter the starlight. In addition to the two targets in this work, another isolated B[e] star, MWC 623 (Lee et al. 2016), has similar dust characteristics determined by polarization technique (Zickgraf & Schulte-Ladbeck 1989).

Miroshnichenko (2007) proposed a binary origin hypothesis for most unclB[e] objects, so a new category of star known as FS CMa stars (FS CMa = HD 45677) was proposed in their study. Our two targets were included in the list of FS CMa-type stars. However, Patel et al. (2006) suggested that the polarization variability of HD 45677 is not likely due to binarity. However, this binary origin hypothesis is inclusive receiving both supporting (Baines et al. 2006; Jeřábková et al. 2016) and contradicting evidence (Corporon & Lagrange 1999; Kluska et al. 2016). Nevertheless, close binaries are expected to be frequently identified among OB stars (Bastian et al. 2010). Polarization variability may be attributable to gas and dust enhancing or forming from a mass transfer environment surrounding a close pair.

6. Conclusions

We perform multicolor and multiepoch polarimetric diagnostics of two isolated B[e] stars, HD 45677 and HD 50138, with the circumstellar dust forming in situ. Their intrinsic polarization is derived on the basis of the measurements of field stars to estimate the IPS contribution. The improved ISP removal necessitated that we reanalyze the observed polarization reported in the literature to obtain a more consistent interpretation of the intrinsic polarization behavior. Consolidating our observations from 2010–2011 with data from the literature reveals the

Table 6
Estimated ISP Values at 340 pc of HD 50138 and 601 pc of HD 45677 Using Four Criteria

Criterion	Q_{ISP} (%)	U_{ISP} (%)	P_{ISP} (%)	θ_{ISP} (°)	No of Stars
			For HD 45677		
I	−0.23 ± 0.19	0.23 ± 0.11	0.33 ± 0.15	67.6 ± 13.4	16
II	−0.27 ± 0.15	0.16 ± 0.06	0.31 ± 0.14	74.7 ± 8.6	8
III	−0.11 ± 0.06	0.27 ± 0.08	0.29 ± 0.07	55.8 ± 5.8	27
IV	−0.22 ± 0.10	0.13 ± 0.06	0.26 ± 0.10	74.4 ± 8.5	10
			For HD 50138		
I	−0.45 ± 0.16	0.66 ± 0.20	0.80 ± 0.19	62.2 ± 6.3	25
II	−0.45 ± 0.17	0.62 ± 0.19	0.76 ± 0.18	63.0 ± 6.7	16
III	−0.25 ± 0.10	0.60 ± 0.16	0.65 ± 0.16	56.2 ± 4.9	27
IV	−0.46 ± 0.17	0.68 ± 0.21	0.82 ± 0.19	62.2 ± 6.3	22

dominant role played by electron scattering in the immediate stellar vicinity in the otherwise dusty envelopes of B[e] stars. Despite the electron scattering, the dust scattering features appear at some epochs of both targets, indicating the existence of in situ dust during these epochs, before leaving outward with the stellar wind from the inner part of the disk. Simultaneous spectroscopic, photometric, and polarimetric observations in the optical and infrared can further elucidate the detailed temporal and positional correlations between stellar mass loss, dust formation, and forbidden line formation in these elusive stars.

This work was initiated by the Taiwan-India Project supported from the National Science Council of Taiwan (NSC 99-2923-M-008-002-MY3). The following financial support from the grants including funded by the Ministry of Science and Technology of Taiwan: (i) MOST 103-2112-M-008-024-MY3, and (ii) MOST 102-2119-M-007-004-MY3, 105-2119-M-007-024, and 106-2119-M-007-021-MY3.

Appendix
ISP Estimations with Different Sets of Field Stars

HD 45677 and HD 50138 are angular and linearly close; thus, we compared the ISPs derived by the field stars within four given field regions with different criteria. Each criterion is described as follows (see also Figure 2):

Criterion I uses all the field stars within a 10° radius of each target, including the overlapping region and non-overlapping region.

Criterion II uses the field stars in the non-overlapping region of the 10° radius for each target (i.e., 11 field stars in the overlapping region were excluded).

Criterion III uses only one common 10° field enclosing both targets. This field centered around the middle point of our two targets.

Criterion IV uses the independent field stars of each target that are separated by a boundary as depicted with a green line in Figure 2.

For each criterion, we followed procedures similar to those mentioned in Section 3.2 to estimate the ISP values at the distances of our targets. Table 6 lists the derived ISP Stokes parameters (Q_V and U_V) and polarizations (P_V and θ_V) along with their uncertainties, as well as the number of stars used for each criterion. We also plot these ISP estimations together in Figure 9. For all four criteria, HD 45677 has similar P_{ISP} and θ_{ISP}; HD 50138 also has comparable P_{ISP} and θ_{ISP} for the three criteria except Criterion III. Considering both targets together, θ_{ISP} of HD 50138 using Criterion III is similar to θ_{ISP} of HD 45677 using any of the four criteria. This suggests that these derived ISP values for HD 50138 are biased by those of HD 45677. Therefore, Criterion III is unreliable.

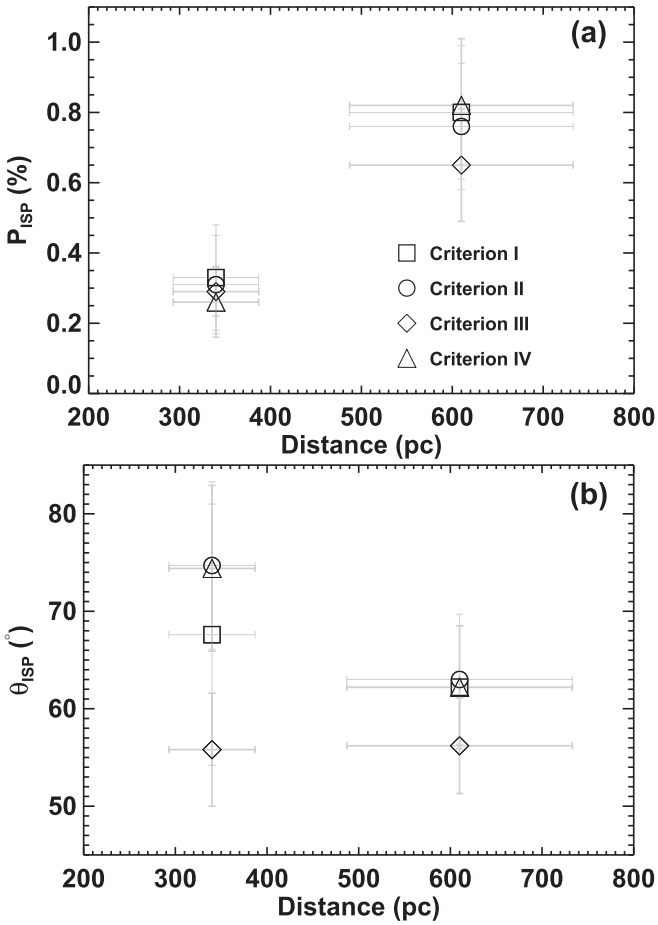

Figure 9. Distance vs. (a) P_{ISP} and (b) θ_{ISP} values derived at the distances of HD 50138 (340 pc) and HD 45677 (610 pc) using the four criteria mentioned in the text. ISP values derived using different criteria are indicated with different symbols denoted in panel (a). Error bars for the *x*-axis are identical to the distance uncertainties of B[e] stars.

Furthermore, Criterion I may yield biased ISP values for HD 50138, because it uses a greater number of common field stars located very close to HD 45677. Criterion II may not yield reliable ISP values because of the omitted field stars that are located close to our targets. To avoid any bias resulting from the using of common stars, we evenly bisect the overlapping region by using a straight line to connect two intersections of

two circles. Figure 2 shows that the field stars from the two sides of this "line" possess different polarization angles. Hence, Criterion IV yields more reliable ISP values. Therefore, we used this criterion to derive intrinsic polarization from the observed polarization in this work.

ORCID iDs

C. D. Lee https://orcid.org/0000-0002-3142-7299
C. Eswaraiah https://orcid.org/0000-0003-4761-6139
W. P. Chen https://orcid.org/0000-0003-0262-272X

References

Allen, D. A. 1973, MNRAS, 161, 145
Ammons, S. M., Robinson, S. E., Strader, J., et al. 2006, ApJ, 638, 1004
Baines, D., Oudmaijer, R. D., Porter, J. M., & Pozzo, M. 2006, MNRAS, 367, 737
Barbier, R., & Swings, J. P. 1982, in IAU Symp. 98, Be Stars, ed. M. Jaschek & H.-G. Groth (Dordrecht: Reidel), 103
Bastian, N., Covey, K. R., & Meyer, M. R. 2010, ARA&A, 48, 339
Bjorkman, K. S. 1991, in European Southern Observatory Conf. and Workshop Proc. 36, ed. D. Baade (Garching: ESO), 101
Bjorkman, K. S., Miroshnichenko, A. S., Bjorkman, J. E., et al. 1998, ApJ, 509, 904
Bjorkman, K. S., Nordsieck, K. H., Code, A. D., et al. 1991, ApJL, 383, L67
Borges Fernandes, M., Kraus, M., Chesneau, O., et al. 2009, A&A, 508, 309
Borges Fernandes, M., Meilland, A., Bendjoya, P., et al. 2011, A&A, 528, A20
Burbidge, E. M., & Burbidge, G. R. 1954, ApJ, 119, 501
Carciofi, A. C., Magalhães, A. M., Leister, N. V., Bjorkman, J. E., & Levenhagen, R. S. 2007, ApJL, 671, L49
Corporon, P., & Lagrange, A.-M. 1999, A&AS, 136, 429
Coyne, G. V., & Kruszewski, A. 1969, AJ, 74, 528
Coyne, G. V., & Vrba, F. J. 1976, ApJ, 207, 790
de Winter, D., & van den Ancker, M. E. 1997, A&AS, 121, 275
Draper, Z. H., Wisniewski, J. P., Bjorkman, K. S., et al. 2014, ApJ, 786, 120
Ellerbroek, L. E., Benisty, M., Kraus, S., et al. 2015, A&A, 573, A77
ESA 1997, in ESA Special Publication, The Hipparcos and Tycho catalogues (Noordwijk: ESA), 1200
Eswaraiah, C., Pandey, A. K., Maheswar, G., et al. 2011, MNRAS, 411, 1418
Gaia Collaboration, Prusti, T., de Bruijne, J. H. J., et al. 2016, A&A, 595, A1
Gnedin, Y. N., Kiselev, N. N., Pogodin, M. A., Rosenbush, A. E., & Rosenbush, V. K. 1992, SvAL, 18, 182
Halonen, R. J., & Jones, C. E. 2013, ApJ, 765, 17
Harrington, D. M., & Kuhn, J. R. 2009, ApJS, 180, 138
Heiles, C. 2000, AJ, 119, 923
Houk, N., & Smith-Moore, M. 1988, Catalogue of Two-dimensional Spectral Types for the HD Stars, Vol. 4 (Ann Arbor, MI: Univ. Michigan Press)
Houziaux, L., & Quinet, P. 2001, in ASP Conf. Ser. 242, Eta Carinae and Other Mysterious Stars: The Hidden Opportunities of Emission Spectroscopy, ed. T. R. Gull, S. Johannson, & K. Davidson (San Francisco, CA: ASP), 213
Humason, M. L., & Merrill, P. W. 1921, PASP, 33, 112
Jaschek, C., & Andrillat, Y. 1998, A&AS, 128, 475
Jeřábková, T., Korčáková, D., Miroshnichenko, A., et al. 2016, A&A, 586, A116
Johnson, H. L. 1958, LowOB, 4, 37
Kluska, J., Benisty, M., Soulez, F., et al. 2016, A&A, 591, A82
Lamers, H. J. G. L. M., Zickgraf, F.-J., de Winter, D., Houziaux, L., & Zorec, J. 1998, A&A, 340, 117
Lee, C.-D., Chen, W.-P., & Liu, S.-Y. 2016, A&A, 592, A130
Leonard, D. C., & Filippenko, A. V. 2005, in ASP Conf. Ser. 342, 1604–2004: Supernovae as Cosmological Lighthouses, ed. M. Turatto et al. (San Francisco, CA: ASP), 330
Magalhaes, A. M. 1992, ApJ, 398, 286
Magalhães, A. M., Melgarejo, R., Pereyra, A., & Carciofi, A. C. 2006, in ASP Conf. Ser. 355, Stars with the B[e] Phenomenon (San Francisco, CA: ASP), 147
McDavid, D. 2001, ApJ, 553, 1027
Medhi, B. J., Maheswar, G., Brijesh, K., et al. 2007, MNRAS, 378, 881
Medhi, B. J., Maheswar, G., Pandey, J. C., Kumar, T. S., & Sagar, R. 2008, MNRAS, 388, 105
Medhi, B. J., Maheswar, G., Pandey, J. C., Tamura, M., & Sagar, R. 2010, MNRAS, 403, 1577
Melgarejo, R., Magalhães, A. M., Carciofi, A. C., & Rodrigues, C. V. 2001, A&A, 377, 581
Merrill, P. W. 1949, PASP, 61, 38
Miroshnichenko, A. S. 2007, ApJ, 667, 497
Miroshnichenko, A. S., Bernabei, S., Bjorkman, K. S., et al. 2006, in ASP Conf. Ser. 355, Stars with the B[e] Phenomenon (San Francisco, CA: ASP), 315
Monnier, J. D., Berger, J.-P., Millan-Gabet, R., et al. 2006, ApJ, 647, 444
Monnier, J. D., Tuthill, P. G., Ireland, M., et al. 2009, ApJ, 700, 491
Niemczura, E., Morel, T., & Aerts, C. 2009, A&A, 506, 213
Oudmaijer, R. D., & Drew, J. E. 1999, MNRAS, 305, 166
Pandey, J. C., Medhi, B. J., Sagar, R., & Pandey, A. K. 2009, MNRAS, 396, 1004
Patel, M., Oudmaijer, R. D., Vink, J. S., Mottram, J. C., & Davies, B. 2006, MNRAS, 373, 1641
Pecaut, M. J., Mamajek, E. E., & Bubar, E. J. 2012, ApJ, 746, 154
Pereyra, A., de Araújo, F. X., Magalhães, A. M., Borges Fernandes, M., & Domiciano de Souza, A. 2009, A&A, 508, 1337
Pickering, E. C., Fleming, W. P., & Cannon, A. J. 1898, ApJ, 8
Poeckert, R., Bastien, P., & Landstreet, J. D. 1979, AJ, 84, 812
Ramaprakash, A. N., Gupta, R., Sen, A. K., & Tandon, S. N. 1998, A&AS, 128, 369
Rautela, B. S., Joshi, G. C., & Pandey, J. C. 2004, BASI, 32, 159
Rivinius, T., Carciofi, A. C., & Martayan, C. 2013, A&ARv, 21, 69
Rodríguez, L. F., Báez-Rubio, A., & Miroshnichenko, A. S. 2012, RMxAA, 48, 47
Schmidt, G. D., Elston, R., & Lupie, O. L. 1992, AJ, 104, 1563
Schmidt-Kaler, Th. 1982, in Landolt-Böstein: Numerical Data and Functional Relationships in Science and Technology, ed. K. Schaifers & H. H. Voigt (Berlin: Springer), 19
Schulte-Ladbeck, R. E. 1994, Ap&SS, 221, 347
Schulte-Ladbeck, R. E., & Clayton, G. C. 1993, AJ, 106, 790
Schulte-Ladbeck, R. E., Shepherd, D. S., Nordsieck, K. H., et al. 1992, ApJL, 401, L105
Serkowski, K., Mathewson, D. S., & Ford, V. L. 1975, ApJ, 196, 261
Stauffer, J. B., & Hartmann, L. W. 1986, PASP, 98, 1233
Swings, J.-P. 1977, Msngr, 8, 10
van Leeuwen, F. 2007, A&A, 474, 653
Whittet, D. C. B., Martin, P. G., Hough, J. H., et al. 1992, ApJ, 386, 562
Wisniewski, J. P., Bjorkman, K. S., Magalhães, A. M., et al. 2007, ApJ, 671, 2040
Wisniewski, J. P., Draper, Z. H., Bjorkman, K. S., et al. 2010, ApJ, 709, 1306
Wood, K., Bjorkman, K. S., & Bjorkman, J. E. 1997, ApJ, 477, 926
Yudin, R. V., & Evans, A. 1998, A&AS, 131, 401
Zickgraf, F.-J., & Schulte-Ladbeck, R. E. 1989, A&A, 214, 274
Zickgraf, F.-J., Wolf, B., Stahl, O., Leitherer, C., & Klare, G. 1985, A&A, 143, 421